ADVANCED FUNCTIONAL MATERIALS

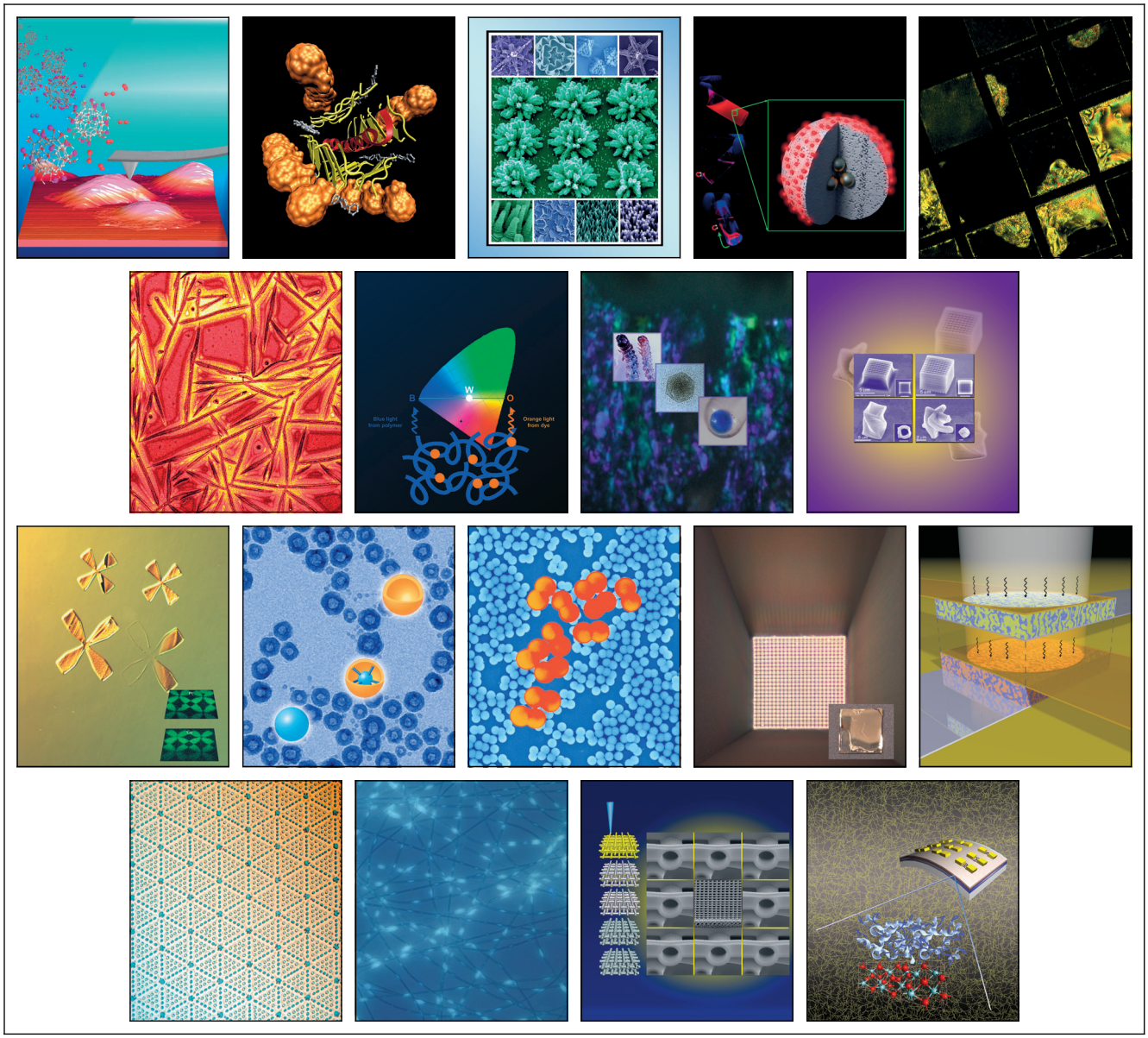

WILEY-VCH

Reprint

ADVANCED FUNCTIONAL MATERIALS

FULL PAPER

DOI: 10.1002/adfm.200600926

New Insights on Near-Infrared Emitters Based on Er-quinolinolate Complexes: Synthesis, Characterization, Structural, and Photophysical Properties**

By *Flavia Artizzu*, *Luciano Marchiò*, *Maria Laura Mercuri*, *Luca Pilia*, *Angela Serpe*, *Francesco Quochi*, *Riccardo Orrù*, *Fabrizio Cordella*, *Michele Saba*, *Andrea Mura*, *Giovanni Bongiovanni*, and *Paola Deplano**

Erbium quinolinolates, commonly assumed to be mononuclear species with octahedral co-ordination geometry, have been proposed as promising materials for photonic devices but difficulties in obtaining well defined products have so far limited their use. We report here the conditions to obtain in high yields three different kinds of pure neutral erbium quinolinolates by mixing an erbium salt with 8-quinolinol (HQ) and 5,7-dihalo-8-quinolinol (H5,7XQ: X = Cl and Br): i) the trinuclear complex Er_3Q_9 (**1**) which is obtained with HQ deprotonated by NH_3 in water or ethanol/water mixtures; ii) the already known dimeric complexes based on the unit $[Er(5,7XQ)_3(H_2O)_2]$ [X = Cl (**2**) and Br (**3**)]; iii) the mononuclear $[Er(5,7XQ)_2(H5,7XQ)_2Cl]$ [X = Cl (**4**) and Br (**5**)] complexes, obtained in organic solvents without base addition, where the ion results coordinated to four ligands, two deprotonated chelating, and two as zwitterionic monodentate oxygen donors. These results represent a further progress with respect to a recent reinvestigation on this reaction, which has shown that obtaining pure and anhydrous octahedral ErQ_3, the expected reaction product, is virtually impossible, but failed in the isolation of **1** and of the neutral tetrakis species based on H5,7XQ ligands. Structural data provide a detailed description of the molecules and of their packing which involves short contacts between quinoxaline ligands, due to π–π interactions. Electronic and vibrational studies allow to select the fingerprints to distinguish the different products and to identify the presence of water. The structure/property relationship furnishes a satisfactory interpretation of the photo-physical properties. Experimental evidence confirms that the most important quenchers for the erbium emission are the coordinated water molecules and shows that the ligand emission is significantly affected by the π–π interactions.

1. Introduction

Since the first report by Tang and VanSlyke[1–3] of efficient electroluminescence from aluminium quinolinolates (AlQ_3 Q = 8-quinolinolate), extensive work has been performed to improve the properties of organic light emitting diodes (OLEDs) till the development of flat panel displays and other emissive devices.[4–6] Rare-earth quinolinolates were synthesized to be used as low cost emitting materials in the near-infrared region.[7–11] Several rare-earth ions emit in the NIR region, and among them Er^{3+} plays a special role since doped silica fibers are currently at the heart of the optical amplification technology used in the long-haul communication systems operating in the 1.5 μm spectral window. Emission arises from electronic transitions between the 4f orbitals, which being symmetry forbidden give rise to weak absorptions. Moreover inorganic erbium salts have very low solubility in all matrices, resulting in long and expensive amplifiers. To overcome these problems the erbium ion is encapsulated by an organic ligand, which should provide a high coordination number preferred by the ion to form a stable complex suitable to be further processed and to shield the ion from additional coordination from the solvent or impurities in the matrix, which can quench the lumines-

[*] Prof. P. Deplano, F. Artizzu, Prof. M. L. Mercuri, Dr. L. Pilia, Dr. A. Serpe
Dipartimento di Chimica Inorganica e Analitica, Università di Cagliari
Cittadella di Monserrato, 09042, Monserrato, Cagliari (Italy)
E-mail: deplano@unica.it
Dr. L. Marchiò
Dipartimento di Chimica Generale ed Inorganica, Chimica Analitica Chimica Fisica, Università di Parma
Parco Area delle Scienze 17A, 43100 Parma (Italy)
Dr. F. Quochi, R. Orrù, F. Cordella, Dr. M. Saba, Prof. A. Mura, Prof. G. Bongiovanni
Dipartimento di Fisica, Università di Cagliari
Cittadella di Monserrato, 09042, Monserrato, Cagliari (Italy)

[**] The "Fondazione Banco di Sardegna" and the MIUR through the PRIN project 2005033820_002 "Molecular materials with magnetic, optical and electrical properties ...", and FIRB projects (Synergy-FIRBRBNE03S7XZ and FIRB-RBAU01N449) are gratefully acknowledged for supporting this research. Crystallographic data (excluding structure factors) for the structures reported in this paper have been deposited with the Cambridge Crystallographic Data Centre as supplementary publication no. CCDC 615603, CCDC 615604, CCDC 615603. Copies of the data can be obtained free of charge from www.ccdc.cam.ac.uk/conts/retrieving.html or on application to The Director: Cambridge Crystallographic Data Centre (CCDC), 12 Union Road, Cambridge CB2 1EZ, UK. Supporting Information is available online from Wiley InterScience or from the authors.

cence. Among the several organo-erbium complexes extensively investigated to overcome these problems in the last decade, the ErQ_3 complex has gathered much attention especially after the demonstration of the first electrically excited organic IR emitter.[7,8] The Q-ligand works as antenna chromophore which sensitizes the ion by intramolecular energy transfer. In addition this ligand may have the potential for electrical pumping. However, photoluminescent studies on ErQ_3 and on complexes with similar ligands have shown lifetimes much shorter (in the 2 μs range) than the natural radiative lifetime of the Er^{3+} $^4I_{13/2} \rightarrow {}^4I_{15/2}$ transition (14 ms). This was ascribed to the presence of CH of the Q-ligand and OH groups eventually present in the solvent (including water), supposed to be the most important IR quenchers.[12–15] This implies that the Q ligand is unable to protect the ion from further coordination by solvent or moisture. To enhance the emission efficiency of ErQ_3 the corresponding complexes with 5,7-halogen substituted Q have been studied.[10,16] The emission efficiency remains, however, very low ($< 10^{-3}$). The reason of this low quantum yield claimed for a quantitative understanding of IR quenching mechanisms in these materials. Despite the interest of physicists into these compounds, since recently their structures were not available, and the interpretation of experimental results was relied on the common assumption of a rare-earth mononuclear structure with octahedral coordination geometry.[17–21] Recently a reinvestigation of the synthetic procedures of rare earth complexes of 8-hydroxyquinoline and its halogen-substituted derivatives has been performed by ourselves[22] and by Van Deun group[23] independently but with the same goal to deepen the knowledge of the chemistry of these complexes, so far limited by experimental difficulties in obtaining analytically pure products and by the absence of structural characterization. Our efforts are focused in finding detailed experimental conditions to provide pure products useful for optical devices and in determining the structural features and properties of these complexes with the aim to find a reliable structure-property relationship.

We report here a study which definitely shows that by reacting an erbium salt with Q, the ligand deprotonated by a suitable base such as NH_3, the *trinuclear* complex Er_3Q_9 is obtained instead of the mononuclear ErQ_3 species commonly assumed. Mononuclear complexes $Er(5,7XQ)_3 \cdot 2H_2O$ (X = Cl and Br) are instead obtained under the same conditions by using H5,7XQ = 5,7-dihalo-8-quinolinol, as previously shown.[23] In addition new mononuclear $[Er(5,7XQ)_2(H5,7XQ)_2Cl]$ complexes, where the erbium is coordinated to four ligands (only two deprotonated) and to one chloride, are obtained by mixing the erbium chloride with H5,7XQ in organic solvents without addition of any base.

The spectroscopic results are presented to deepen the knowledge of the electronic and vibrational features of the ligands and complexes and also to furnish simple tools which can help in distinguishing the different coordination modes in the complexes, whether or not the ligands are present in deprotonated or protonated form, whether or not water is present. Moreover the emissive properties of these products are investigated applying a reliable quantitative description of the non-radiative decay processes induced by the dipolar coupling between CH groups and the lanthanide ion[24] recently proposed by us.[25]

2. Results and Discussion

2.1. Synthesis and Crystal Structure Description

In Scheme 1a summary of the synthetic procedures used to obtain three different kinds of neutral erbium complexes in high yields is reported. As shown apparently small differences in the reactions' conditions produce different products: i) the

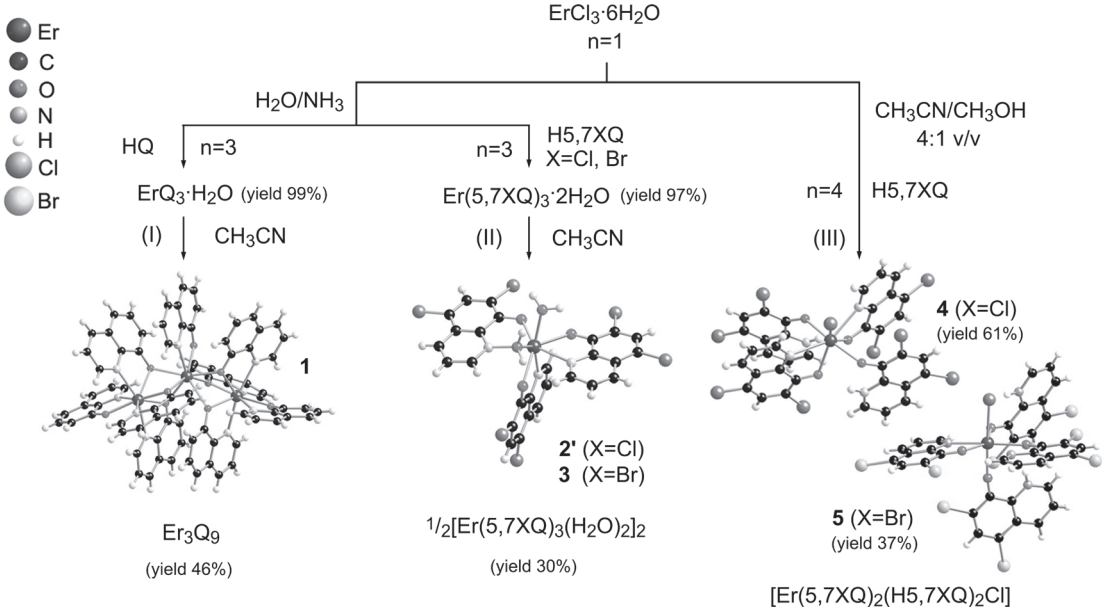

Scheme 1. Reaction pathways.

ADVANCED FUNCTIONAL MATERIALS

trinuclear complex Er_3Q_9 (**1**) which is obtained when Q is the unsubstitued ligand deprotonated by NH_3 either in water or ethanol/water mixtures; ii) the dimeric complexes where the mononuclear unit consists of $[Er(5,7XQ)_3(H_2O)_2]$ [X = Cl (**2**) and Br (**3**)] where the ion is octacoordinated to three deprotonated ligands and to two water molecules, when 5,7XQ is 5,7-dihalo-8-quinolinol; iii) the mononuclear $[Er(5,7XQ)_2(H5,7XQ)_2Cl]$ [X = Cl (**4**) and Br (**5**)] complexes, where only two of the four coordinated ligands are deprotonated, obtained by mixing the erbium chloride with H5,7XQ in organic solvents without addition of any base.

The pathway I of Scheme 1 follows a slight modification of the most conventional literature procedure reported to obtain the assumed to be ErQ_3.[26] Accordingly, as described in detail in the Experimental part, few drops of NH_3 28 % were added to a HQ in H_2O mixture under mixing (Scheme 1, pathway I). After 30 min a water solution of $Er(NO_3)_3 \cdot 5H_2O$ or $ErCl_3 \cdot 6H_2O$ (in the 3:1 ligand to metal molar ratio) was added to the above mixture, which is allowed to react for two days. A yellow precipitate is formed, collected by filtration, washed with water, NaOH 0.1 M, water and dried in oven. Elemental analysis on this solid is in agreement with an $ErQ_3 \cdot H_2O$ formulation. The same product is obtained by using ethanol (or methanol) to dissolve HQ and erbium chloride in spite of the nitrato salt. Suitable crystals for a diffractometric X-ray study were obtained on re-crystallization of the crude product from warm CH_3CN. Structural results show that the obtained product is a *trinuclear* species $Er_3Q_9 \cdot CH_3CN$ (**1**), as reported in reference 22. A similar trinuclear structure is exhibited also by $[Ho_3Q_9] \cdot HQ$.[27] The ESI-Mass Spectra of the crude product analyzed as $ErQ_3 \cdot H_2O$ and of $Er_3Q_9 \cdot CH_3CN$ show the presence of $Er_3Q_8^+$ cation in both samples showing that the trinuclear structure is the reaction product, that is not formed on recrystallization in organic solvents, and that is preserved in solution. In reference [23] the corresponding reaction in water is reported to produce crude products with analytical results in agreement with a metal to ligand ratio 1:3, ESI-mass corresponding to $Ln_3Q_8^+$ and ^{1}HNMR spectra showing more peaks than expected for a LnQ_3 formulation. However, the crystals isolated by using ethanol as solvent showed to be $NH_4[Er_3Q_8Cl(OH)] \cdot 4C_4H_8O_2$. On the basis of the reported experimental details, it may be suggested that the crude products of reference [23] correspond to Er_3Q_9 (ESI-Mass Spectra and analytical results match perfectly with our findings). The fact that $NH_4[Er_3Q_8Cl(OH)] \cdot 4C_4H_8O_2$ was isolated in ethanol in spite of **1**, may be related to the reaction times (10 min) shorter with respect to those used in our experiments to collect Er_3Q_9. Low soluble ionic intermediates can precipitate in organic solvents before the reaction is gone to completion.

The molecular structure of **1** has been shortly described previously.[22] Each metal presents a distorted square anti-prismatic geometry with the two outer metals bound by four nitrogen and four oxygen atoms whereas the inner erbium is octacoordinated by a nitrogen and seven oxygen atoms. The crystal packing reveals the presence of partial π stack between adjacent trinuclear complexes involving quinoxaline ligand with interligand spacings in the 3.307–3.407 Å range (see Fig. S1 in the Supporting Information).

By using as ligand 5,7-dihalo-8-quinolinol (H5,7ClQ) and (H5,7BrQ), the reaction described above produces $[Er(5,7ClQ)_3(H_2O)_2]$ (**2**), and $[Er(5,7BrQ)_3(H_2O)_2]$ (**3**), (Scheme 1, pathway II) which on recrystallization from warm CH_3CN do not lose the water molecules, that are coordinated to the erbium ion. The crystal structure shows that the two octa-coordinated units shown in Scheme 1 form a dimer through four hydrogen bonds $[Er(5,7ClQ)_3(H_2O)_2]_2 \cdot 3H_2O \cdot CH_3CN$ (**2′**) (Fig. S2 in the Supporting Information). **2′** differs from the dimer described in reference [23] for the non-coordinated solvent molecules. Intermolecular interactions involve quinoxaline ligand with interligand spacings in the 3.41–3.6 Å range.

When the 5,7-halosubstituted ligands (H5,7XQ, X = Cl, Br) are reacted in the absence of NH_3 and in organic solvents (CH_3CN/CH_3OH 4:1 mixtures) with erbium chloride tetrakis neutral species are obtained (Scheme 1, pathway III). Crystals of $[Er(5,7XQ)_2(H5,7XQ)_2Cl]$ (X = Cl (**4**); X = Br (**5**)), suitable for X-ray diffractometric studies have been obtained. The ion results epta-coordinated to four ligands, two N,O chelated in deprotonated form as anions, and two can be formally considered as zwitterionic ligands (N^+–H and O^-) and therefore act as monodentate oxygen donors. The charge of the metal ion is balanced by one coordinating halogenide. In the unit cell of **4**, two independent molecules are present, which are related by a *pseudo* center of symmetry, Figure 1. The two independent molecules interact through a partial stack between the III-VIII and IV-VII quinoline molecules with the minimum distance between these stacks of 3.422(8) (C(93)···C(108)) and 3.439(8) Å (C(97)···C(104)). A summary of X-ray crystallographic data for **2′**, **4**, and **5** is reported in Table 1. Selected bond lengths of compounds **2′**, **4**, **5** are reported in Table 2.

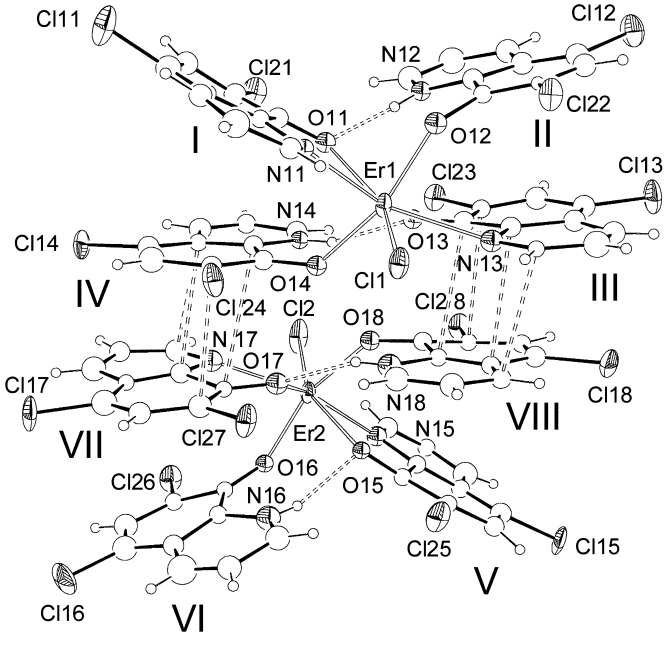

Figure 1. Ortep drawing of $[Er(5,7ClQ)_2(H5,7ClQ)_2Cl]$ (**4**) at the 30 % ellipsoids level. Roman numbers refer to the quinoline molecules.

Table 1. Summary of X-ray crystallographic data for **2′**, **4**, and **5**.

	2'	**4**	**5**
Empirical formula	$C_{28}H_{20.50}Cl_6ErN_{3.50}O_{6.50}$	$C_{72}H_{36}Cl_{18}Er_2N_8O_8$	$C_{38}H_{21}Br_8ClErN_5O_4$
Formula weight	889.94	2113.71	1453.59
Colour, habit	Yellow, Block	Orange, Block	Orange, block
Crystal size, mm	0.10x0.10x0.05	0.10x0.08x0.05	0.55x0.35x0.25
Crystal system	Trigonal	Orthorhombic	Monoclinic
Space group	R-3	Pca21	P21/c
a, Å	21.679(1)	25.570(9)	13.493(9)
b, Å	21.679(1)	9.750(7)	17.295(9)
c, Å	37.224(2)	29.490(9)	18.151(9)
α, deg.	90	90	90
β, deg.	90	90	97.16(3)
γ, deg.	120	90	90
V, Å^3	15150(1)	7352(6)	4203(4)
Z	18	4	4
T, K	293	293	293
ρ(calc), Mg/m^3	1.756	1.910	2.297
μ, mm^{-1}	3.016	2.985	9.713
θ range, deg.	1.64 to 26.05	1.38 to 24.02	3.05 to 25.00
No.of rflcn/obsv F>4σ(F)	53113 / 3391	34926 / 4465	7580 / 4096
GooF	1.011	0.929	1.001
R1 [a]	0.0361	0.0659	0.0655
wR2 [b]	0.0546	0.1123	0.1414

[a] $R1 = \Sigma||F_o|-|F_c||/\Sigma|F_o|$. [b] $wR2 = [\Sigma[w(F_o^2-F_c^2)^2]/\Sigma[w(F_o^2)^2]]^{1/2}$; $w = 1/[\sigma^2(F_o^2) + (aP)^2 + bP]$, where $P = [\max(F_o^2,0) + 2F_c^2]/3$.

Table 2. Selected bond lengths [Å] for **2′**,**4**, **5**.

	2′		
Er-N(11)	2.542(5)	**Er-O(11)**	2.287(4)
Er-N(12)	2.500(5)	**Er-O(12)**	2.317(4)
Er-N(13)	2.449(4)	**Er-O(13)**	2.296(4)
Er-O1w	2.364(4)	**Er-O2w**	2.414(4)
	4		
Er(1)-O(11)	2.26(2)	**Er(2)-O(15)**	2.37(2)
Er(1)-O(12)	2.12(2)	**Er(2)-O(16)**	2.20(2)
Er(1)-O(13)	2.36(2)	**Er(2)-O(17)**	2.24(2)
Er(1)-O(14)	2.12(2)	**Er(2)-O(18)**	2.16(2)
Er(1)-N(11)	2.48(2)	**Er(2)-N(15)**	2.52(2)
Er(1)-N(13)	2.50(2)	**Er(2)-N(17)**	2.56(2)
Er(1)-Cl(1)	2.611(7)	**Er(2)-Cl(2)**	2.621(7)
	5		
Er-O(11)	2.316(8)	**Er-N(11)**	2.52(1)
Er-O(12)	2.182(8)	**Er-N(14)**	2.478(9)
Er-O(13)	2.294(8)	**Er-Cl**	2.687(3)
Er-O(14)	2.223(8)		

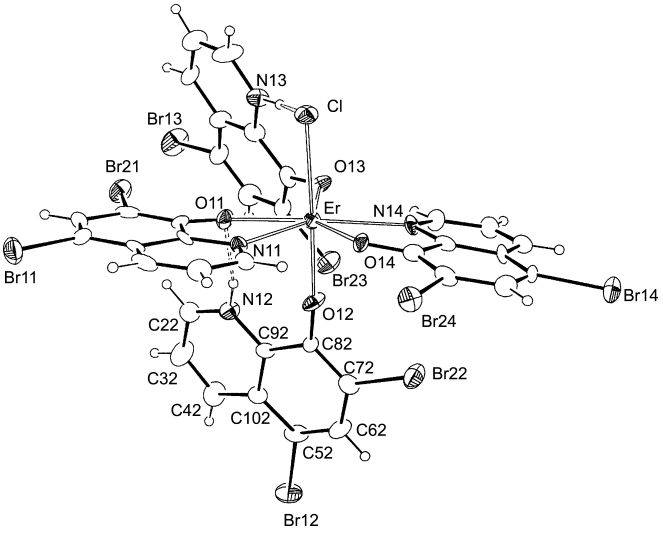

Figure 2. Ortep drawing of $[Er(5,7BrQ)_2(H5,7BrQ)_2Cl]\cdot CH_3CN$ (**5**) at the 30% ellipsoids level. The CH_3CN solvent molecule has been removed for clarity.

The coordination geometry of **4** and **5** can be described as distorted pentagonal bipyramidal with the equatorial positions defined by Cl(1)-O(11)-O(13)-N(11)-N(13) for Er(1) in **4**, Cl(2)-O(15)-O(17)-N(15)-N(17) for Er(2) in **4** and O(11)-O(13)-O(14)-N(11)-N(14) for Er in **5**, Figure 2. The molecular geometry of **4** and **5** differs in the spatial disposition of the quinoline molecules with respect to each other and in the hydrogen bonds that the protonated quinolines (N^+–H as hydrogen bond donor) exchange with the surrounding groups. In **4**, the N–H are directed toward the oxygen atoms of the opposite and N,O chelated quinoline, whereas in **5** one N–H interacts with the chlorine ions and the second with the oxygen atom of a quinoline. Geometric parameters of the hydrogen bonds of **4** and **5** are reported in Table 3. The crystal packing of **4** reveals

Table 3. Geometric parameters of the hydrogen bonds of **4** and **5**.

	d(Å)	N-H···X (deg.)
	4	
N(12) ··O(11)	2.89(3)	154(2)
N(14) ··O(13)	2.91(3)	160(2)
N(16) ··O(15)	2.73(3)	166(2)
N(18) ··O(17)	2.96(3)	162(2)
	5	
N(13) ··Cl	3.10(1)	154.2(7)
N(12) ··O(11)	2.81(1)	167.6(7)

the presence of two interconnected layers in the *ac* and *bc* crystallographic planes, respectively. These layers are determined by the partial stack of I and VI quinoline molecules (*bc* layer) and by the partial stack of the I-VI and II-V quinoline molecules (*ac* layer), Figure 3.

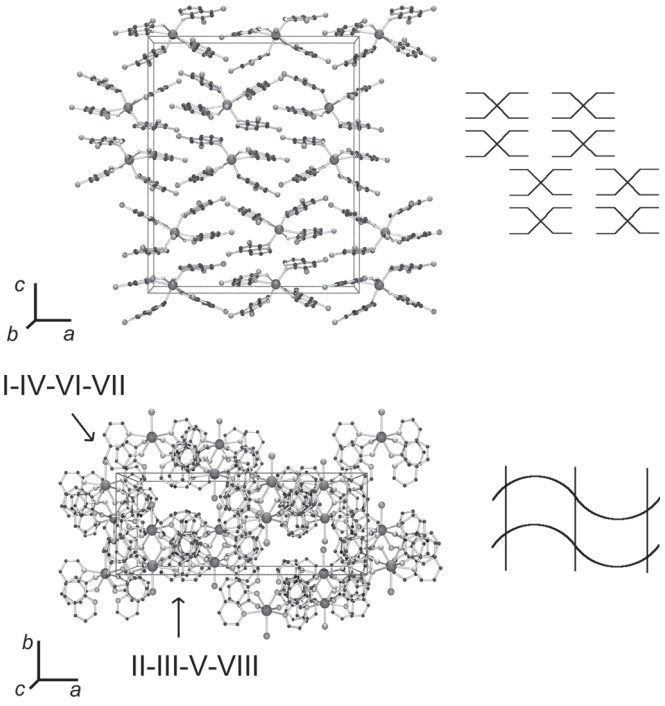

Figure 3. Crystal packing of $[Er(5,7ClQ)_2(H5,7ClQ)_2Cl]$ (**4**) projected along the *b* (above) and *c* (below) crystallographic axes together with a schematic description of the packing.

The crystal packing of **5** is reported in Figure S3 in the Supporting Information. A partial π stack that involves the quinoxaline moieties is in the 3.36–3.69 Å range.

The reported results suggest that three main factors are important in determining the nature of obtained products: 1) the tendency of the erbium ion to reach high coordination numbers; 2) the steric and 3) electronic factors induced by substituents in the quinoline ligand. Accordingly, the capability of Q to work as bridging ligand allow the erbium ion to achieve the preferred coordination number 8, also in the presence of only three ligand molecules for ion in the trinuclear form **1**. The reason why 5,7-halo substituted Q do not work as bridging ligands, can be relatable to the steric hindrance of the halogens at the 7 position which gives rise to an energy barrier in reaching the trinuclear form, as proposed by Van Deun.[23] In addition it must be taken into account that the presence of 5,7-halo-substituents affects the electronic distribution in the quinoline ring, stabilizing the anionic form and producing higher acidity with respect to the unsubstitued Q. This may explain the production of $[Er(5,7XQ)_2(H5,7XQ)_2Cl]$ by mixing the reagents without any base addition.

2.2. Spectroscopic Studies

2.2.1. Electronic Spectroscopy

The ligands of the complexes under discussion belong to the well known family of 8-hydroxyquinolinate which are emitters used generally coordinated to metals, the most often used is Al^{3+}, where the metal ion has the role of improving the stability and the efficiency of the emitting material.[2] In the cases under discussion the ligands work as "antenna" molecules, where the HOMO-LUMO energy separation matches the intra-atomic transition of the erbium emitting ions. Moreover the ligand in the complexes plays the important role of electron-transport material, when used in OLED devices.[4–6]

The electronic spectra of the ligands, either in neutral or in deprotonated form, and of complexes are reported in Figures 4 and 5. The lowest energy absorption band is red shifted in the anion, and this shift is higher for the halogen-substituted li-

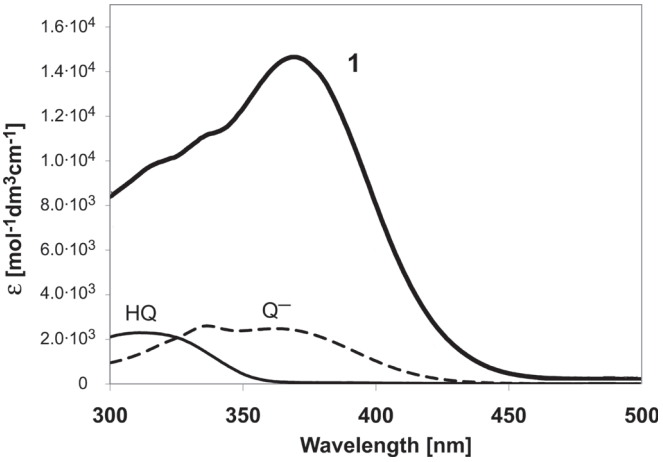

Figure 4. UV-visible spectrum of **1** in MeOH solution. The spectra of the ligand are reported for comparison.

gands. This peak is further red-shifted in the complexes, to an extent comparable to that generally observed in complexes with closed-shell metal ions while the shift is larger and sensitive to the metal in complexes with open-shell transition metals.[28] Moreover this band is red shifted as the polarity of the solvent increases. Approximate calculations based on semiempirical extended Hückel methods have been performed by

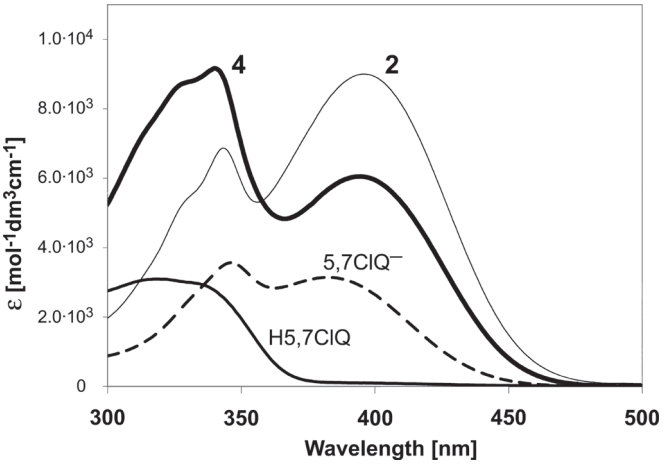

Figure 5. Uv-visible spectra of **2** and **4** in MeOH solution. The spectra of the ligand are reported for comparison.

using the CACAO program.[29] The frontier orbitals of Er_3Q_9, and those of Q^- in the insert, are shown in Figure 6.

In the ligands, as expected, the HOMO and LUMO are π orbitals. The phenoxidic ring gives an increasing higher contribution to the HOMO and the pyridinic one the LUMO with the introduction of the halogen atoms at the 5,7 position of Q. This gives an increasing charge-transfer character to the HOMO-LUMO transition with a consequent increase in the absorptivities, as observed. Moreover the strongly antibonding character of the carbon-halogen bonds in the HOMO pushes up in energy this orbital as the population of the halogen atom increases (Br > Cl) but the antibonding character of the carbon-halogen bonds is weaker in the LUMO. This explains the observed red shift of the $\pi \rightarrow \pi^*$ transition in the halo-substituted ligands. In the erbium-complexes the frontier orbitals consist of set of closely spaced orbitals which preserve the electronic structure of the individual ligands with no significant contribution from the erbium ion. As an example in **1** nine closely spaced HOMOs and nine LUMOs are found, and in Figure 6 the highest energy HOMO and the third LUMO are shown to compare with the frontier orbitals of the free ligand. These findings while based on approximate calculations give a simplified description useful for a rough explanation of the observed spectral features.

The diffuse reflectance (DR) spectra of **1**, **2′**, and **4** are reported in Figures 7–9 The DR spectra performed on microcrystalline powders dispersed on Teflon film allow to identify the ligand centered transitions as well as the sharp $f \rightarrow f$ erbium bands which are assigned according to literature.[30,31] While most of these peaks are affected little by the coordination around the lanthanide ion, the peak near 520 nm shows different intensities in the different complexes. This peak is known as the hypersensitive band[32] and its increase in intensity is related to the increase of the oscillator strength of the $^4I_{15/2} \rightarrow {}^4H_{11/2}$ pseudo-quadrupolar transition as a consequence of a lowering of the symmetry in the coordination sphere. In **1** the relative intensity of this peak referred to the 975 nm one is almost double than that found in erbium chloride[33] whose

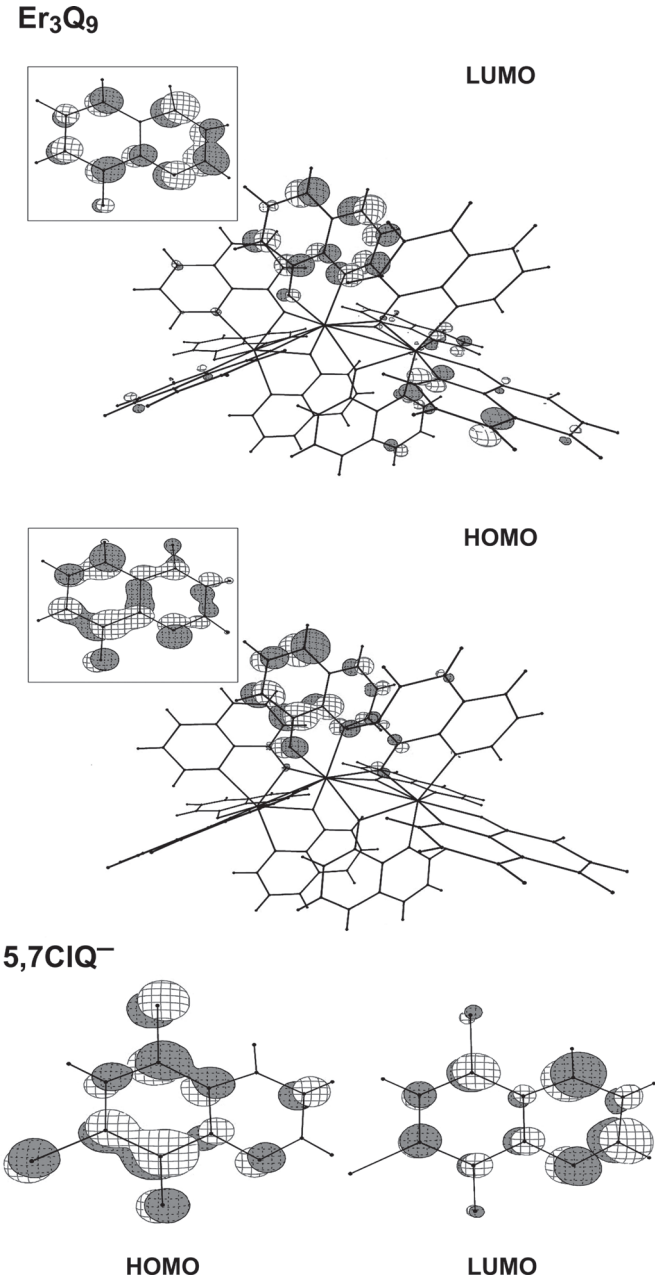

Figure 6. Frontier Molecular Orbitals in the free ligands and as an example in **1**, calculated by using semi-empirical extended Hückel methods through the CACAO program.

structure is shown in Figure S4 in the Supporting Information, reflecting the lower symmetrical environment around the ion.

In **2′** and **3** in the solid state the peak at 521 nm is weaker than in **1**, while in **4** and **5** is covered by an additional shoulder near 480 nm that could be assigned to a $\pi \rightarrow \pi^*$ intermolecular transition due to the stacking, which is particularly effective in these complexes.

The near infrared region is relevant to find experimental evidence for the presence of IR quenchers responsible for the undesired shortening of the natural radiative lifetime of the Er^{3+} $^4I_{13/2} \rightarrow {}^4I_{15/2}$ transition near 1500 nm. This transition is split in

ADVANCED FUNCTIONAL MATERIALS

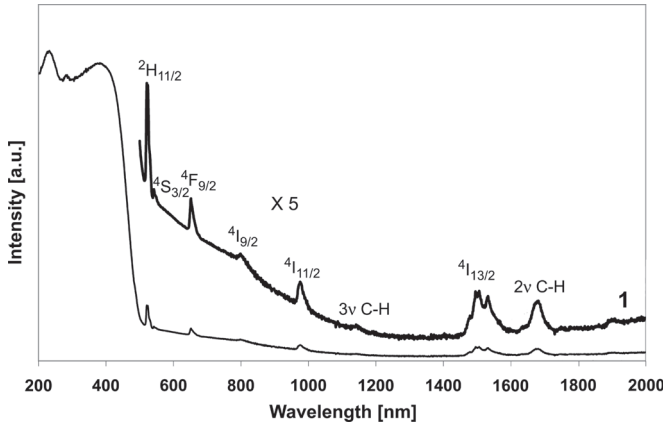

Figure 7. Diffuse reflectance spectrum of **1**, showing the f–f peaks and the overtones of CH stretchings.

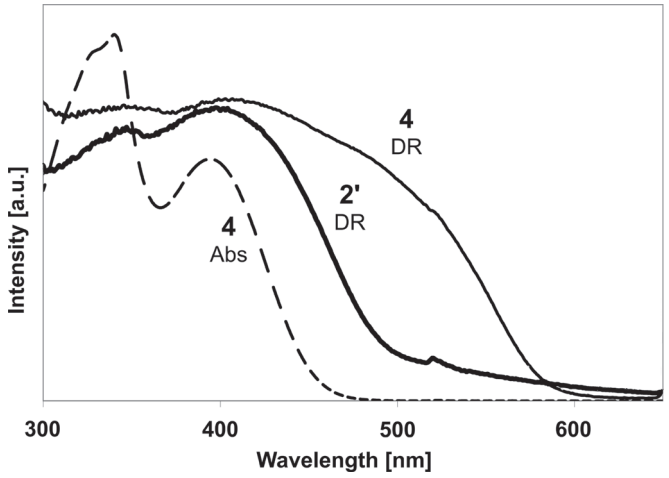

Figure 8. Diffuse reflectance spectra of **2′** and **4** (continuous lines). For comparison the MeOH solution spectrum of **4** (dashed line) is reported.

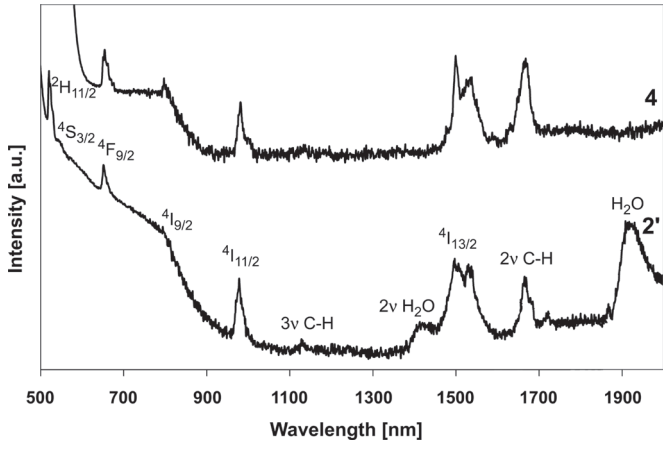

Figure 9. Diffuse reflectance spectra of **4** and **2′**, showing the f–f peaks and the overtones of OH stretchings in H_2O (1920 $a\nu_1 + \nu_2 + b\nu_3$, ν_1 symmetric, ν_3 antisymmetric stretching and ν_2 bending; 1420 $\nu_1 + \nu_3$).

all the complexes. The splitting is relatable to a partial removal of the degeneration of the involved levels as a consequence of the asymmetry of the local field induced by the coordination (Stark splitting).[6]

In **1**–**5** the first and second overtones of the aromatic C–H stretching vibrations appear near 1675 nm and 1140 nm respectively. Instead the presence of water molecules is unambiguously identified in **2′** and **3** only through the peaks near 1920 and 1420 nm assigned to the combination bands $a\nu_1 + \nu_2 + b\nu_3$ and $\nu_1 + \nu_3$, respectively (ν_1 and ν_3 = symmetrical and antisymmetrical stretching; ν_2 = bending of the HOH group). The presence of the peaks near 1420 and 1675 nm, partially overlapping the emission peak, gives experimental evidence to take into account the quenching processes of the erbium emission. These data coupled with structural results have crucial importance for a quantitative study of the emission properties. Moreover, the identification of water through DR spectra on microcrystalline samples dispersed on a Teflon film has shown to be more reliable compared to the assignment through conventional infrared spectroscopy on samples dispersed as KBr pellets, being KBr easily contaminated by the ubiquitous presence of water.

2.2.2. Vibrational Spectroscopy

The vibrational spectra of quinolinolato-metal complexes, including lanthanide derivatives, have been reported since long time.[34–36] Recently more sophisticated theoretical studies, including *ab initio* calculations, have furnished reliable assignments on AlQ_3.[37] Based on these previous studies the FT-infrared and -Raman spectra of **1**–**5** are discussed. The samples share the following common features: the aromatic CH vibrations near 3050 cm^{-1}, the ring stretching in the 1620–1300 cm^{-1} range, the CO stretching near 1100 cm^{-1}. Below 1000 cm^{-1} the CH wagging and ring deformation modes appear. A ring breathing mode and a ring deformation are found near 740 and 500 cm^{-1}, respectively. The comparison of the infrared spectra of **2** and **4** (and similarly of **3** and **5**) allows to identify in **4**, additional peaks which are relatable to the ligand protonated as pyridinium (3200, 1620, 1311 cm^{-1}), see Figure S5 in the Supporting Information. Moreover the splitting of the peaks due to CO stretching and ring breathing near 1100 and 740 cm^{-1} reflects the unequivalence of the coordinated ligands. Similar information are drawn by the comparison of Raman spectra. An interesting sequence of combination bands of the ring vibrations is found in the 2900–2700 cm^{-1} region. These combination bands are more intense in **1**, **4**, and **5** where several π–π intermolecular interactions are present with an overlapping of the rings more effective than in **2** where only a partial stacking and no combination bands are observed. Figure S6 in the Supporting Information.

2.2.3. Photoluminescence Studies

In this paragraph, we discuss the excited-state dynamics and light emission properties of Er-complexes. A simplified energy level scheme of the organolanthanides is reported in Figure 10. After optical excitation, singlet states S_1 can either decay to the ground state S_0, or to triplet states T_1. These latter excita-

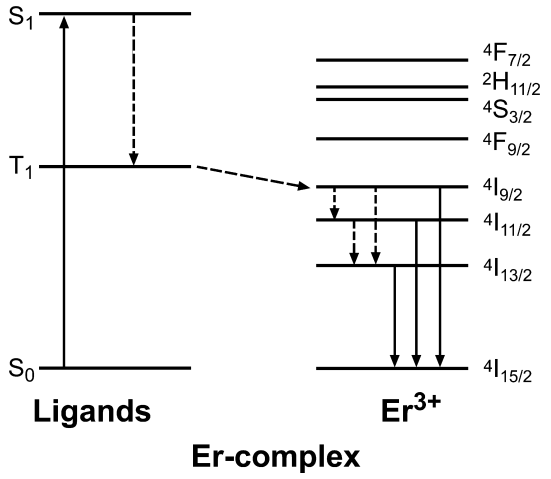

Figure 10. Jablonski diagram depicting excited-state relaxation and NIR emission in Er-complexes. The singlet states S_1 are excited through the absorption of one photon. Downward arrows show relaxation channels, including radiative (continuous lines) and nonradiative (dashed lines) decay pathways. The long-dashed arrow indicates energy transfer from the ligand to the Er-ion.

tions can subsequently transfer to the metal. Following a fast excited-state ion relaxation, the radiative decay $^4I_{13/2} \rightarrow {}^4I_{15/2}$ yields the NIR emission at 1.54 μm.

Figure 11 shows the luminescence spectra in the visible spectral region of **1**, **2′**, and **4** excited at 390 nm. Emission bands are assigned to the $S_1 \rightarrow S_0$ transitions of the ligand. The spectra of the trinuclear species **1**, and of the tetrakis complex **4** in solution are similar, featuring an unstructured band peaked at 520 nm. The large Stokes-shift from the absorption maximum at 370–400 nm arises from the fast geometrical relaxation following excitation of the S_1 state.[38] In crystals with tetrakis molecular arrangement, the emission is shifted to longer wavelength (620 nm) with respect to the tris complex **2′**. This finding confirms the redshift observed in the DR spectra,

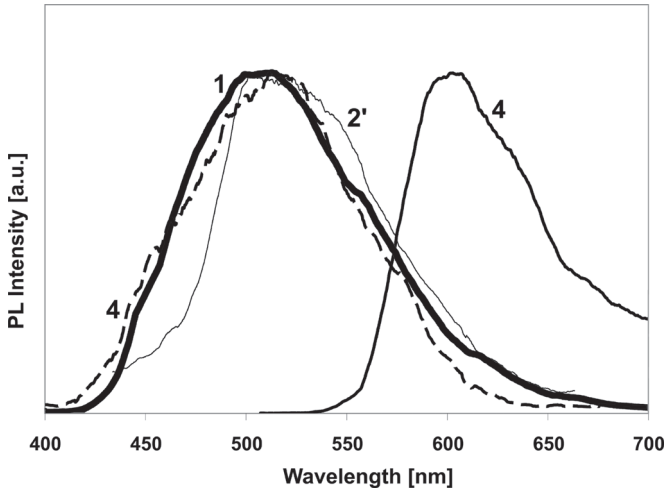

Figure 11. Photoluminescence spectra of trinuclear complex **1** (DMSO solution), tris complex **2′** (crystals) and of the tetrakis complex **4** in the solid state (solid line) and in DMSO solution (dashed line).

which was ascribed to the peculiar π–π intermolecular interactions of the tetrakis crystal structure.[39a] The influence of the isomeric states and of the packing on the fluorescence wavelengths of AlQ_3 compounds has been also investigated.[39b] As expected, the redshift of the emission to 620 nm does not occur in the tetrakis complexes in solution, Figure 11.

Representative photoluminescence spectra in the NIR are depicted in Figure 12. The spontaneous emission reveals the same Stark-split transitions reported in the DR optical re-

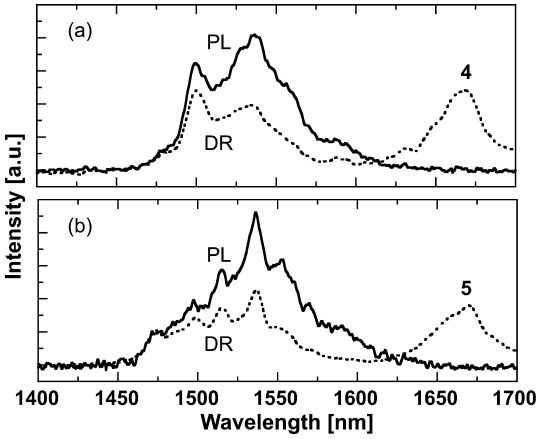

Figure 12. Photoluminescence (continuous line) and diffuse reflectance (dashed line) spectra of **4** (panel a) and **5** (panel b).

sponse. The relative line intensities differ slightly: the lower energy transitions of the photoluminescence spectra are more intense due to efficient electron thermalization, which favors the occupation of the lower energy states of the $^4I_{13/2}$ manifold.

Excited-state relaxation dynamics is investigated by looking at the time evolution of the luminescence of the ligand and the phosphorescence of the Er^{3+} ions. Complexes are excited by 200 fs-long-pulses at 390 nm. Visible emission is detected by a 2D-streak-camera with a rise-time of 10 ps, while spectrally integrated NIR emission has been selected by low energy band-pass filters and detected by an amplified photodiode with 2-ns resolution.

Figure 13 shows that the intensity of the singlet luminescence of the quinoline ligands in Er-complexes decays with characteristic times ranging from 10 to 40 ps both in crystals and in solution. This fast radiative relaxation should be compared with that observed in complexes with lighter ions, as AlQ_3, which are characterized by a nanosecond decay time. The short singlet lifetime in organolanthanides is thus ascribed to the very efficient spin-triplet conversion due to the presence of the lanthanide ion, which enhances the spin-orbit coupling (heavy-atom effect).

At later delays, the excitation energy of triplet states in the ligand can transfer to the erbium ion. This process is monitored by studying the build up of the NIR emission from the rare-earth. Experimental results are reported in Figure 14. The transient phosphorescence signal reveals a fast peak-response at time equal to zero, followed by a slower decay. A spectral

ADVANCED FUNCTIONAL MATERIALS

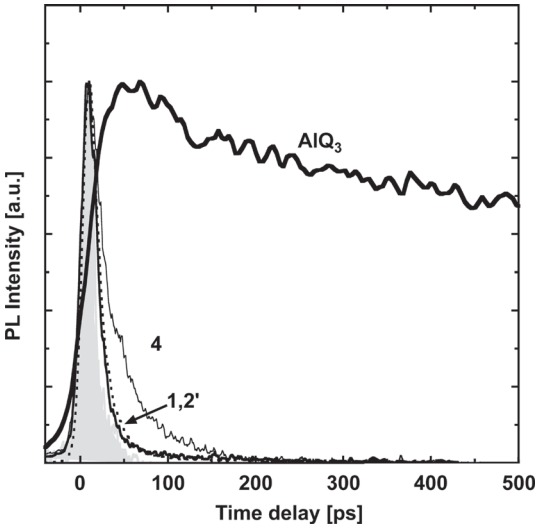

Figure 13. Spectral integrated vis-photoluminescence decay traces of trinuclear complex **1** (dotted line, solution), tris-complexes **2′** and AlQ_3 (crystals), tetrakis complex **4** (crystals). The shaded gray curve represents the temporal response of the streak camera to fs-pulses.

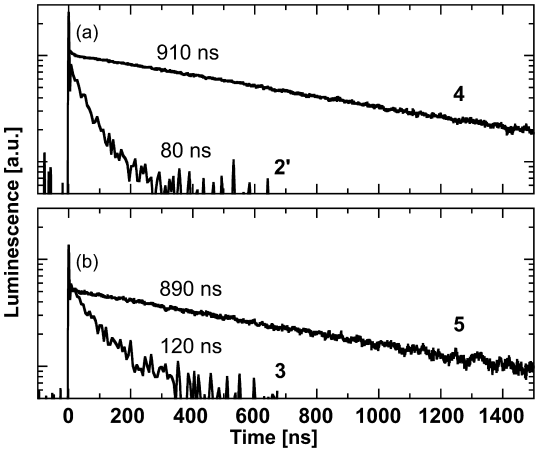

Figure 14. NIR-photoluminescence decay traces of **4** and **2′** (panel a), **5** and **3** (panel b) crystals. The peak at time equal to zero arises from the radiative decay at 980 nm of the $^4I_{11/2}$ state, which is transiently populated during energy relaxation in the lanthanide ion. Such peak is not visible in the traces of **4** and **5**, for which the detection bandwidth was reduced from 1 GHz to 20 MHz. The slower signal stems from the radiative decay at 1540 nm of the $^4I_{13/2}$ state.

analysis shows that the former signal arises from the radiative decay at 980 nm from the $^4I_{11/2}$ level, which is transiently populated during energy relaxation. The slower signal stems from the radiative decay at 1540 nm of the $^4I_{13/2}$ state. The signal risetime is limited by the time resolution of the experimental apparatus, which fixes an upper limit of ~2 ns to the energy transfer time to the rare-earth. Since the characteristic triplet lifetime of the ligand is much longer, these data indicate that most of the triplet population is transferred to the lanthanide.

The analysis of the time-resolved photoluminescence signal supports the conclusion that the two-step process $S_1 \rightarrow T_1 \rightarrow Er^{3+}$ is the dominant excited-state relaxation pathway of the lanthanide complexes. The low quantum yield of the NIR emission should be thereby primarily caused by the nonradiative decay of the ion excitation. Both CH groups and water are responsible for the NIR emission quenching. Water molecules in the first coordination sphere of the Ln^{3+}-ion are, however, expected to lead to a much faster nonradiative decay rate. This effect is clearly observed in Figure 14, where the emission decay is reported for complexes with (**2′** and **3**) and without (**4** and **5**) water molecules. In water-free compounds, the nonradiative lifetime falls in the μs time-scale, in agreement with previous experimental and theoretical investigations.[22,25] In hydrated complexes, interaction with the vibrations of water shortens the excited-state lifetime down to ~80–120 ns. The efficient quenching induced by water molecules can be quantitatively accounted for by assuming a dipolar coupling between the excited states of the Ln^{3+} ion and the high frequency water vibration at 1420 nm. It must be remarked that this vibration is a combination of the symmetrical and antisymmetrical stretchings of OH groups in water, thus it will be absent in compound containing isolated OH groups. In the framework of the Förster's energy transfer resonant theory,[24] a theoretical nonradiative lifetime of ~100 ns is estimated using the spectroscopic and structural data of the hydrated complexes. The fast decay induced by water molecules results from: (i) the shorter Er^{3+}-OH_2 distance, (ii) the larger transition dipole of the OH combination overtone, and (iii) the better fulfillment of the resonance condition between the Er and OH vibrational dipoles.

3. Conclusions

In conclusion we have pointed out the conditions to obtain in high yields pure trinuclear and tetrakis neutral erbium quinolinolate complexes. These results seem particularly relevant taking into account that physicists still prepare[40] erbium quinolinolate complexes following literature methods or a slightly modification of that, which are expected wrongly to produce ErQ_3 mononuclear species with octahedral coordination geometry. The invoked ErQ_3 has been used as emitting material deposited by vacuum deposition either on quartz glass for photoluminescence studies[20] or on a silicon substrate[19] or on indium-tin-oxide coated glass[7,18] in the production of OLEDs emitting electroluminescence at 1.5 μm. The same material has been processed incorporated in a polymer host as a thin-film blend in polycarbonate.[17] Our results represent a further progress with respect to a recent reinvestigation on this reaction, which has shown that obtaining pure and anhydrous octahedral ErQ_3 is virtually impossible, but failed in the isolation of the formed compound **1**, the trinuclear species Er_3Q_9. In addition we have found the conditions to prepare in high yields new neutral pure tetrakis complexes and have confirmed that $[ErQ_3 \cdot 2H_2O]_2$ is obtained in the halosubstituted case only. The difficult item to obtain neutral pure products, since impure products are detrimental for applications in optical devices, and neutral compounds are preferable with respect to ionic ones for processing purposes, has been overcome by this study.

The structural data provide a detailed description of the molecules and of their different packing which involves well-defined short contacts between quinolinolate ligands, due to π–π orbital overlaps. The investigation of the electronic and vibrational properties of the different complexes allows to select the most significant fingerprints to distinguish the different products, to identify the presence of water and to achieve a deep understanding of the obtained samples. Experimental evidence has confirmed that the most important quenchers for the erbium emission are the coordinated water molecules. The structural characterization of the products allows also to find a satisfactory structure/property relationship for the interpretation of the photo-physical properties and for designing new complexes with improved luminescence.

4. Experimental

Chemicals: All the reagents and solvents were purchased from Aldrich and used without further purification.

*$Er_3Q_9 \cdot CH_3CN$ (**1**): Method A*: Few drops of NH_3 28 % up to a final concentration of 2.0×10^{-2} mol dm^{-3} (pH ≃ 10) were added to a mixture of 8-hydroxy-quinoline (0.157 g, 1.08 mmol) in H_2O (100 mL) under mixing. (Caution must be taken in controlling the NH_3 amount in order to avoid its excess which can induce the precipitation of the very unsoluble erbium hydroxide.) After 30 min a water solution of $Er(NO_3)_3 \cdot 5H_2O$ (0.160 g, 0.361 mmol) was added to the above mixture which is allowed to react for 2 days until the white solid due to the unreacted ligand disappears. A yellow precipitate is formed, collected by filtration, washed with water, NaOH 0.1 M to improve the solubility of the free ligand eventually present, water, and dried in oven at 120 °C (almost quantitative yield). Analytical results are in agreement with the $ErQ_3 \cdot H_2O$ formulation. CHN Found (Calculated) for $C_{27}H_{20}ErN_3O_4$: C % 52.31(52.50), H % 3.22(3.26), N % 6.96(6.80). The solid was then dissolved in warm CH_3CN, the solvent was roto-evaporated to incipient precipitation and after several days yellow crystals of pure $Er_3Q_9 \cdot CH_3CN$ were obtained (yield 46 %). CHN Found (Calcd for $C_{83}H_{57}Er_3N_{10}O_9$): C % 53.75(54.07); H % 3.45(3.50); N % 7.07(7.01). *Method B*: $ErCl_3 \cdot 6H_2O$ (0. 159 g, 0.359 mmol) was dissolved in 30 mL of methanol (or ethanol) and the resulting solution was slowly added to 100 mL of a solution of 8-hydroxy-quinoline (0.156 g, 1.075 mmol) in the same solvent. Afterwards, few drops of NH_3 28 % were added to the reaction mixture and the resulting solution was maintained under stirring at room temperature for several days until a yellow solid precipitated. The obtained product was washed with NaOH 0.1 M, water and dried in oven (almost quantitative yield). Analytical results are in agreement with the $ErQ_3 \cdot 2H_2O$ formulation. CHN Found (Calculated) for $C_{27}H_{22}ErN_3O_5$: C % 51.12(51.01), H % 3.44(3.49), N % 6.82(6.61). The solid was then recrystallized from CH_3CN and the experimental data of the obtained crystals are in agreement with the $Er_3Q_9 \cdot CH_3CN$ formulation. ESI-Mass (CH_3CN/CH_3OH 3/1): *m/z* 1654.98 [$Er_3Q_8^+$]. FT-IR spectrum (cm^{-1}): 3047 m, 2957 vw, 2928 vw (*ν*CH, CH_3CN), 2786 vw, 2697 vw, 2647 vw, 2562 vw, 1917 vw, 1601 m, 1571 s, 1498 vs, 1466 vs, 1424 mw, 1383 s, 1318 s, 1276 m, 1231 m, 1174 w, 1108 vs, 1035 w (*δ* C–H), 905 w, 823 m, 804 m, 787 m, 732 s, 648 m, 606 m, 592 w; 571 w, 504 m, 489 m, 384 m, 361 m, 309 w, 210 s, 162 m, 144 w, 115 w, 70 w. FT-Raman spectrum (cm^{-1}): 3065 m, 2936 m, 2895 m, 2764 m, 1584 m, 1424 w, 1372 s, 1331 w, 1283 w, 1135 w, 1064 m, 905 w, 738 m, 504 m, 282 w, 140 m. UV-vis spectrum (nm; [$dm^3\,mol^{-1}\,cm^{-1}$]): 369[$(1.47 \pm 0.03) \times 10^4$], 521[< 17]. DR spectrum (nm): 227, 277 sh, 384, 521, 541, 652, 799, 977, 1501–1531, 1679.

*$[Er(5,7ClQ)_3(H_2O)_2]_2 \cdot 3H_2O \cdot CH_3CN$ (**2'**)*: Few drops of NH_3 28 % were added to a mixture of 5,7-dichloro-8-quinolinol (0.230 g, 1.075 mmol) in H_2O (150 mL) and the mixture was maintained under vigorous stirring at 35 °C. After 60 min a water solution of $Er(NO_3)_3 \cdot 5H_2O$ (0.159 g, 0.359 mmol) was added and after few days of stirring at room temperature a dark-yellow precipitate was collected, washed with water, NaOH 0.1 M, water, and dried in oven at 120 °C (yield 97 %). CHN: Found (Calcd for $Er(5,7ClQ)_3 \cdot 3H_2O$ **(2)**): C % 37.54(37.69), H % 2.20(2.11), N % 5.02(4.88). The solid was dissolved in hot CH_3CN and the resulting solution was concentrated up to half volume and then left standing to the air. After several days dark-yellow crystals suitable for X-ray studies were collected (yield 30 %). CHN: Found (Calcd for $C_{28}H_{20.50}Cl_6ErN_{3.50}O_{6.50}$ **(2')**) C % 37.88(37.79), H % 2.27(2.32), N % 5.47(5.51). FT-IR spectrum (cm^{-1}): 3074 w, 2928 w (*ν*CH, CH_3CN), 1594 w, 1560 s, 1491 s, 1452 vs, 1395 m, 1376 s, 1286 w, 1251 mw, 1234 mw, 1195 w, 1141 w, 1111 m, 1053 w (*δ* C–H), 1028 vw, 961 m (*ν*C–Cl), 884 m (*ν*C–Cl), 809 mw, 788 mw, 751 s, 671 m, 649 mw, 586 w, 507 vw, 418 mw. FT-Raman spectrum (cm^{-1}): 3071 m, 2936 mw, 2257 w, 1576 m, 1493 w, 1457 vw, 1364 vs, 1290 w, 1140 w, 1054 w, 961 vw, 755 mw, 649 w, 590 w, 503 m, 412 m, 348 m, 246 m, 204 m, 177 m, 148 m. UV-vis spectrum (nm; [$dm^3\,mol^{-1}\,cm^{-1}$]): 343[$(6.9 \pm 0.1) \times 10^3$], 396[$(9.0 \pm 0.1) \times 10^3$], 521[< 10]. DR spectrum (nm): 266, 348, 400, 520, 653, 803, 975, 1497–1527, 1667.

*$Er(5,7BrQ)_3(H_2O)_2$ (**3**)*: The synthesis was carried out following the procedure described above, adding a water solution of $ErCl_3 \cdot 5H_2O$ (0.130 g, 0.340 mmol) to a mixture of 5,7-dibromo-8-quinolinol (0.309 g, 1.020 mmol) in H_2O (150 mL) made slightly basic by the addition of few drops of NH_3 28 % (yield 97 %). CHN: Found (Calcd for $Er(5,7BrQ)_3 \cdot 3H_2O$): C % 29.05 (28.77), H % 1.20(1.61), N % 3.79(3.73). The solid was recrystallized in hot CH_3CN. After several days yellow crystals were collected (yield 30 %). Experimental data are in agreement with the $Er(5,7BrQ)_3(H_2O)_2$ formulation. CHN: Found (Calcd for $C_{83}H_{39}Br_{18}Er_3N_{10}O_9$) C % 30.30(29.24), H % 1.17(1.45), N % 4.21(3.79). FT-IR spectrum (cm^{-1}): 3071 w, 1554 s, 1485 s, 1453 vs, 1391 s, 1372 s, 1274 w, 1248 mw, 1217 mw, 1202 w, 1138 mw, 1108 m, 1050 mw (*δ* C–H), 938 m (*ν*C–Br), 860 m (*ν*C–Br), 809 m, 786 m, 744 s, 686 m, 667 m, 654 w, 641 mw; 625 vw, 595 w, 568 m, 503 vw, 419 mw, 414 s, 394 s, 361 m, 346 m, 243 s, 206 m, 164 m, 146 m, 115 w. FT-Raman spectrum (cm^{-1}): 3068 m, 1567 m, 1486 w 1457 vw, 1359 vs, 1282 w, 1138 w, 1054 w, 942 vw, 750 mw, 641 w, 572 mw, 501 m, 499 m, 348 m, 264 m, 203 m, 152 m, 119 m.UV-vis spectrum (nm; [$dm^3\,mol^{-1}\,cm^{-1}$]): 344[$(7.6 \pm 0.1) \times 10^3$], 397[$(9.1 \pm 0.1) \times 10^3$], 521[< 10]. DR spectrum (nm): 228 sh, 267, 348, 402, 521, 652, 803, 973, 1497–1531, 1669.

*$[Er(5,7ClQ)_2(H5,7ClQ)_2Cl]$ (**4**)*: 0.442 g (2.064 mmol) of 5,7-dichloro-8-quinolinol were dissolved in 150 mL of CH_3CN/CH_3OH (4:1 v/v) at 35–40 °C. $ErCl_3 \cdot 6H_2O$, (0.197 g, 0.516 mmol), dissolved in 10 mL of the same solvent mixture, (this salt is more soluble in organic solvent with respect to the nitrato one) was slowly added to the ligand solution and the reaction mixture turned suddenly yellow. After 24 h the solution was roto-evaporated until it turned orange. After few days red crystals, suitable for X-ray studies, were collected and washed with diethyl ether (yield 61 %). CHN: Found (Calcd for $C_{36}H_{18}Cl_9ErN_4O_4$) C % 40.66(40.91), H % 1.70 (1.72), N % 5.28(5.30). FT-IR spectrum (cm^{-1}): 3236 vw, 3171 vw, 3104 w, 3026 w, 2966 w, 2914 w, 2850 vw, 2752 vw, 2115 w, 2013 w, 1616 m, 1592 w, 1559 s, 1542 m, 1489 m, 1454 vs, 1394 m, 1374 s, 1312 m, 1294 w, 1251 w, 1234 mw, 1220 m, 1193 m, 1144 m, 1112 m (split peak), 1051 mw (*δ* C–H), 991 vw, 957 m (*ν*C–Cl), 876 m (*ν*C–Cl), 810 m, 789 m, 748 s (split peak), 672 m, 659 m, 646 w, 634 m, 586 w, 571 mw, 504 m, 419 mw. FT-Raman spectrum (cm^{-1}): 3068 m, 2887 m, 2730 m, 1592 m, 1594 m, 1555 mw, 1488 w, 1469 mw, 1455 w, 1405 w, 1360 vs, 1317 w, 1292 m, 1254 w, 1215 w, 1144 m, 1115 vw, 1051 m (*δ* C–H), 956 w, 876 w, 761 m, 727 m, 680 w, 646 w, 572 w, 501 m, 407 m, 378 mw, 365 m, 348 mw, 275 w, 205 s, 170 s, 144 s. UV-vis spectrum (nm; [$dm^3\,mol^{-1}\,cm^{-1}$]): 340[$(9.17 \pm 0.05) \times 10^3$], 394[$(6.05 \pm 0.03) \times 10^3$], 521[< 10]. DR spectrum (nm): 237, 290 sh, 358 sh, 410, 521 sh, 654, 799, 981, 1499–1536, 1671.

*$[Er(5,7BrQ)_2(H5,7BrQ)_2Cl] \cdot CH_3CN$ (**5**)*: The synthesis was carried out following the procedure described for the analogous tetrakis complex with H5,7ClQ. A slight excess, in order to avoid the precipitation of the ligand, of $ErCl_3 \cdot 6H_2O$ (0.166 g, 0.434 mmol) dissolved in 10 mL of of CH_3CN/CH_3OH (4:1 v/v.) was slowly added to a solution of 5,7-dibromo-8-quinolinol (0.395 g, 1.304 mmol) in the same solvent mixture. After several days, red crystals, suitable for X-ray studies, were collected and washed with diethyl ether (yield 37 %, calculated with

respect to the ligand). CHN: Found (Calcd for $C_{38}H_{21}Br_8ClErN_5O_4$) C % 30.79(31.40), H % 1.42(1.46), N % 4.76(4.82). FT-IR spectrum (cm^{-1}): 3221 vw, 3143 vw, 3064 w, 2989 vw (νCH, CH_3CN), 2928 vw, 2868 w, 2817 vw, 2734 vw, 2250 vw (νCN, CH_3CN), 2092 w, 1609 m, 1594 m, 1552 vs, 1485 s, 1453 vs, 1389 s, 1368 vs, 1315 m, 1300 mw, 1242 mw, 1217 mw, 1196 mw, 1140 m, 1107 m, 1049 m (δC–H), 1005 vw, 986 vw, 939 m (νC–Br), 909 vw, 884 m, 860 m (νC–Br), 805 m, 789 m, 743 s, 685 s, 668 m, 656 m, 641 mw, 625 m, 595 vw, 569 m, 507 m, 418 mw. FT-Raman spectrum (cm^{-1}): 3068 m, 2933 m, 2886 m, 2801 w, 2724 w, 2250 w, 1590 m, 1567 m, 1486 w, 1460 w, 1492 w, 1361 vs, 1315 w, 1285 w, 1276 w, 1257 w (split peak), 1179 vw, 1140 m, 1110 vw, 1050 m, 810 vw, 752 m, 731 m, 685 w, 640 w, 625 w, 572 w, 559 w, 501 m, 414 m, 338 w, 315 m, 263 m, 208 w, 185 m, 129 s, 108 m. UV-vis spectrum (nm; [$dm^3\,mol^{-1}\,cm^{-1}$]): 342[$(8.21\pm0.10)\times10^3$], 396[$(6.17\pm0.09)\times10^3$], 521[<10]. DR spectrum (nm): 652, 802, 982, 1472, 1498, 1514, 1536, 1669.

Spectroscopy: UV-vis-NIR: Diffuse reflectance (DR) and absorption spectra in CH_3OH solution (10^{-4} mol L^{-1}) were collected with a Varian Cary 5 spectrophotometer. Crystalline samples for DR spectra were dispersed on a Teflon film.

IR: FT-IR spectra on KBr pellets were collected with a Bruker Equinox 55 spectrophotometer.

RAMAN: FT-Raman spectra of crystalline samples were collected with a Bruker RFS/100S spectrometer operating in a back-scattering geometry with a Nd:YAG (1064 nm) laser source.

Photoluminescence Studies: Photoluminescence spectra and transients were excited by 1 kHz train of 200 fs-long-pulses at 390 nm. Visible emission was spectrally and temporally dispersed by an imaging polychromator coupled to a 2D-streak camera. At low repetition rate, the signal rise-time is 10 ps. NIR emission was detected using an amplified InGaAs photodiode with a 2-ns response time, and averaged using a digitizing scope with either 20 MHz or 1 GHz detection bandwidth. The laser and visible frequencies were cut using color-glass filters. The NIR emission spectra were recorded using a monochromator coupled to an amplified low-noise InGaAs photodiode.

Data Collection and Structure Determination: A summary of data collection and structure refinement for $[Er(5,7ClQ)_3(H_2O)_2]\cdot 1.5H_2O\cdot 0.5CH_3CN$ (**2′**), $[Er(5,7ClQ)_2(H5,7ClQ)_2Cl]$ (**4**) and $[Er(5,7BrQ)_2(H5,7BrQ)_2Cl]\cdot CH_3CN$ (**5**) is reported in Table 1. Single crystal data was collected with a Bruker AXS Smart 1000 area detector diffractometer (Mo Kα; $\lambda=0.71073$ Å) for **2′**–**4** and with a Philips PW 1100 diffractometer (Mo Kα; $\lambda=0.71073$ Å) for **5**. Cell constants were obtained from a least-square refinement of selected strong reflections distributed over a hemisphere of the reciprocal space (**2**–**4**) [41] and by a least-square refinement of the setting angles of 24 randomly distributed and carefully centered reflections ($6.14<2\theta<16.00$) (**5**). No crystal decay was observed for both compounds. Absorption correction using the program SADABS [42] was applied for **2′**–**4** (min. and max. transmission factors: 0.822–1.000 for **2′**, 0.735 and 1.000 for **4**). An absorption correction using the method of Walker & Stuart [43] was applied for **5** giving transmission factors of 0.873–1.000. The structures were solved by direct methods (SIR97) [44] and refined with full-matrix least squares (SHELXL-97) [45], using the Wingx software package [46]. For **4** only the Er and Cl atoms where refined anisotropically whereas for **2′** and **5** all non-hydrogen atoms were refined anisotropically. The H atoms were placed at their calculated positions. The twin law 100, 010, 00–1 was applied for the refinement of **4**. In the crystal structure of **2**, acetonitrile and water were found disordered with site occupancy factor of 0.5 and 1.5, respectively. The maximum and minimum peaks of the final difference Fourier maps corresponded to 0.986 and –0.352 (**2**), 2.873 and –2.205 (**4**) and 1.228 and –1.217 (**5**) e $Å^{-3}$. Graphical material was prepared with the ORTEP3 for Windows [47] program. Full tables of bond lengths and angles, atomic positional parameters, anisotropic displacement parameters are given in the supplementary material.)

Received: October 6, 2006
Revised: December 14, 2006
Published online: August 15, 2007

[1] C. W. Tang, S. A. VanSlyke, *Appl. Phys. Lett.* **1987**, *51*, 913.
[2] C. H. Chen, J. Shi, *Coord. Chem. Rev.* **1998**, *171*, 161.
[3] C. W. Tang, S. A. VanSlyke, C. H. Chen, *J. Appl. Phys.* **1989**, *65(9)*, 3610.
[4] U. Mitscke, P. Bauerle, *J. Mater. Chem.* **2000**, *10*, 1471.
[5] T. W. Kelley, P. F. Baude, C. Gerlach, D. E. Ender, D. Muyres, M. A. Haase, D. E. Vogel, S. D. Theiss, *Chem. Mater.* **2004**, *16*, 4413.
[6] J. Kido, Y. Okamoto, *Chem. Rev.* **2002**, *102*, 2357.
[7] R. J. Curry, W. P. Gillin, *Appl. Phys. Lett.* **1999**, *75*, 1380.
[8] W. P. Gillin, R. J. Curry, *Appl. Phys. Lett.* **1999**, *74*, 798.
[9] O. M. Khreis, R. J. Curry, M. Somerton, W. P. Gillin, *J. Appl. Phys.* **2000**, *88*, 777.
[10] M. Iwamuro, T. Adachi, Y. Wada, T. Kitamura, S. Yanagida, *Chem. Lett.* **1999**, 539.
[11] O. M. Khreis, W. P. Gillin, M. Somerton, R. J. Curry, *Org. Electron.* **2001**, *2*, 45.
[12] G. Hebbink, *Ph.D. Thesis*, Twente University, The Netherlands **2002**.
[13] M. P. O. Wolbers, F. C. J. M. Van Veggel, B. H. M. Snellink-Ruël, J. W. Hofstraat, F. A. J. Geurts, D. N. Reinhoudt, *J. Chem. Soc. Perkin Trans. 2* **1998**, 2141.
[14] A. Beeby, S. Faulkner, *Chem. Phys. Lett.* **1997**, *266*, 116.
[15] D. Parker, J. A. G. Williams, *J. Chem. Soc. Dalton Trans.* **1996**, 3613.
[16] R. Van Deun, P. Fias, K. Driesen, K. Binnemans, C. Görller-Walrand, *Phys. Chem. Chem. Phys.* **2003**, *5*, 2754.
[17] S. W. Magennis, A. J. Ferguson, T. Bryden, T. S. Jones, A. Beeby, I. D. W. Samuel, *Synth. Met.* **2003**, *138*, 463.
[18] R. J. Curry, W. P. Gillin, *Synth. Met.* **2000**, *111–112*, 35.
[19] R. J. Curry, W. P. Gillin, A. P. Knights, R. Gwilliam, *Opt. Mater.* **2001**, *17*, 161.
[20] J. Thompson, R. I. R. Blyth, G. Gigli, R. Cingolani, *Adv. Funct. Mater.* **2004**, *14*, 979.
[21] R. I. R. Blyth, J. Thompson, Y. Zou, R. Fink, E. Umbach, G. Gigli, R. Cingolani, *Synth. Met.* **2003**, *139*, 207.
[22] F. Artizzu, P. Deplano, L. Marchiò, M. L. Mercuri, L. Pilia, A. Serpe, F. Quochi, R. Orrù, F. Cordella, F. Meinardi, R. Tubino, A. Mura, G. Bongiovanni, *Inorg. Chem.* **2005**, *44*, 840.
[23] R. Van Deun, P. Fias, P. Nockemann, A. Schepers, T. N. Parac-Vogt, K. Van Hecke, L. Van Meervelt, K. Binnemans, *Inorg. Chem.* **2004**, *43*, 8461.
[24] T. Förster, *Discuss. Faraday Soc.* **1959**, *27*, 7.
[25] F. Quochi, R. Orrù, F. Cordella, A. Mura, G. Bongiovanni, F. Artizzu, P. Deplano, M. L. Mercuri, L. Pilia, A. Serpe, *J. Appl. Phys.* **2006**, *99*, 053 520.
[26] H. F. Aly, F. M. Abdel Kerim, A. T. Kandil, *J. Inorg. Nucl. Chem.* **1971**, *33*, 4340.
[27] S. G. Leary, G. B. Deacon, P. C. Junk, *Z. Anorg. Allg. Chem.* **2005**, *631*, 2647.
[28] R. Ballardini, G. Varani, M. T. Indelli, F. Scandola, *Inorg. Chem.* **1986**, *25*, 3858.
[29] C. Mealli, D. Proserpio, *J. Chem. Educ.* **1990**, *67*, 39.
[30] K. Kuriki, Y. Koike, Y. Okamoto, *Chem. Rev.* **2002**, *102*, 2347.
[31] L. H. Slooff, A. Van Blaaderen, A. Polman, G. A. Hebbink, S. I. Klink, F. C. J. M. Van Veggel, D. N. Reinhoudt, J. W. Hofstraat, *Appl. Phys. Lett.* **2002**, *91(7)*, 3955.
[32] S. A. Davis, F. S. Richardson, *Inorg. Chem.* **1984**, *23*, 184.
[33] R. D. Rogers, L. K. Kurihara, *Lanthanide Actinide Res.* **1986**, 296.
[34] A. A. Shabaka, M. Fadly, M. A. El Ghandoor, F. M. Abdel Kerim, *J. Mater. Sci.* **1990**, *25*, 2193.
[35] A. T. Rane, V. V. Ravi, *Spectrochim. Acta Part A* **1982**, *38(8)*, 937.
[36] B. Marchon, L. Bokobza, G. Cote, *Spectrochim. Acta Part A* **1986**, *42(4)*, 537.
[37] M. D. Halls, R. Aroca, *Can. J. Chem.* **1998**, *76*, 1726.
[38] M. Ottonelli, G. Izzo, F. Rizzo, G. Musso, G. Dellepiane, R. Tubino, *J. Phys. Chem. B* **2005**, *109*, 19 249.
[39] a) M. Brinkmann, G. Gadret, M. Muccini, C. Taliani, N. Masciocchi, A. Sironi, *J. Am. Chem. Soc.* **2000**, *122*, 5147. b) H. Kaji, Y. Kusaka, G. Onoyama, F. Horii, *J. Am. Chem. Soc.* **2006**, *128*, 4292.

[40] Y. Li, H. Yang, Z. He, L. Liu, W. Wang, F. Li, L. Xu, *J. Mater. Res.* **2005**, *20*, 2940.
[41] SMART (control) and SAINT (integration) software for CCD systems, Bruker AXS, Madison, WI, USA **1994**.
[42] Area-Detector Absorption Correction; Siemens Industrial Automation, Inc., Madison, WI, USA **1996**.
[43] N. Walker, D. Stuart, *Acta Crystallogr. Sect. A* **1983**, *39*, 158.
[44] A. Altomare, M. C. Burla, M. Camalli, G. L. Cascarano, C. Giacovazzo, A. Guagliardi, A. G. G. Moliterni, G. Polidori, R. Spagna, *J. Appl. Crystallogr.* **1999**, *32*, 115.
[45] G. M. Sheldrick, SHELX97. Programs for Crystal Structure Analysis **1997**, (Release 97-2). University of Göttingen, Germany.
[46] L. J. Farrugia, *J. Appl. Crystallogr.* **1999**, *32*, 837.
[47] L. J. Farrugia, *J. Appl. Crystallogr.* **1997**, *30*, 565.